Journal of Inflammation Research Dovepress

Open Access Full Text Article ORIGINAL RESEARCH

Study on the Anti-Atherosclerotic Mechanisms of Xin-Tong-Tai Granule Through Network Pharmacology, Molecular Docking, and Experimental Validation

Junping Zhu[1–3], Ziyan Wang[4,5], Chengxin Liu[4,5], Min Shi[1,5], Zhihua Guo[1,4,5], Ya Li[2], Rong Yu[1,3], Jiaming Wei[1,5]

[1]School of Chinese Medical Sciences, Hunan University of Chinese Medicine, Changsha, 410208, People's Republic of China; [2]School of Pharmacy, Hunan University of Chinese Medicine, Changsha, 410208, People's Republic of China; [3]Hunan Key Laboratory of TCM Prescription and Syndromes Translational Medicine, Hunan University of Chinese Medicine, Changsha, 410208, People's Republic of China; [4]First Hospital and First Clinical College of Chinese Medicine, Hunan University of Chinese Medicine, Changsha, 410208, People's Republic of China; [5]Hunan Key Laboratory of Colleges and Universities of Intelligent Traditional Chinese Medicine Diagnosis and Preventive Treatment of Chronic Diseases of Hunan Universities of Chinese Medicine, Changsha, 410208, People's Republic of China

Correspondence: Jiaming Wei; Rong Yu, School of Chinese Medical Sciences, Hunan University of Chinese Medicine, 300 Xueshi Road, Science & Technology Industrial Park, Yuelu District, Changsha, Hunan, 410208, People's Republic of China, Email 004916@hnucm.edu.cn; 002165@hnucm.edu.cn

Background: Xin-Tong-Tai Granule (XTTG), a Chinese medicine (CM) formula, has demonstrated significant therapeutic effects on atherosclerosis (AS) in both clinical and experimental settings. Nonetheless, the mechanisms underlying XTTG's efficacy remain largely unexplored. This study aimed to elucidate the mechanisms through which XTTG acts against AS, employing network pharmacology, molecular docking, and experimental validation techniques.

Methods: Initially, target identification for the main chemical components of XTTG was conducted using database, followed by determining the intersection targets between these compounds and disease. Protein-protein interaction (PPI) network analysis, Gene Ontology (GO) enrichment, and Kyoto Encyclopedia of Genes and Genomes (KEGG) pathway analyses were subsequently utilized to investigate the potential pathways through which XTTG exerts its effects on AS. Molecular docking was done to confirm the binding efficacy of XTTG's active components. Additionally, the effects of XTTG were evaluated in vitro using oxidized low-density lipoprotein (ox-LDL) induced human aortic vascular smooth muscle cells (HAVSMCs) and in vivo in apolipoprotein E gene knockout ($ApoE^{-/-}$) mice fed a high-fat diet (HFD).

Results: 229 therapeutic targets were screened for PPI network and enrichment analysis. Notably, the nuclear factor kappa-B (NF-κB) signaling pathway, along with processes related to inflammation and autophagy, were significantly enriched, highlighting their importance. In vitro studies showed that XTTG repressed cell proliferation and lipid droplet aggregation in ox-LDL-induced HAVSMCs. It also decreased the ratio of phosphorylated NF-κB p65/ NF-κB p65, tumor necrosis factor-α (TNF-α) and interleukin-6 (IL-6) levels, and elevated microtubule-associated protein light chain 3 (LC3) and decreased p62 protein expression. In vivo, XTTG ameliorated blood lipid profiles and aortic pathology in HFD-fed $ApoE^{-/-}$ mice, reduced NF-κB p65 expression and serum levels of TNF-α and IL-6, increased the ratio of LC3II/LC3I while decreasing p62 protein expression.

Conclusion: XTTG mitigates AS primarily through anti-inflammatory and autophagy-modulating mechanisms, particularly via inhibition of NF-κB p65 expression. These findings underscore the potential of CM in treating AS and support its further clinical exploration.

Keywords: Xin-Tong-Tai granule, atherosclerosis, network pharmacology, molecular docking, experimental verification

Introduction

Atherosclerosis (AS) is a multifaceted disorder that predominantly targets the major and mid-sized arteries, manifesting as atherosclerotic plaques.[1] This condition can impact all organs and stands as the principal cause of cardiovascular-

Received: 11 September 2024
Accepted: 26 October 2024
Published: 4 November 2024

Graphical Abstract

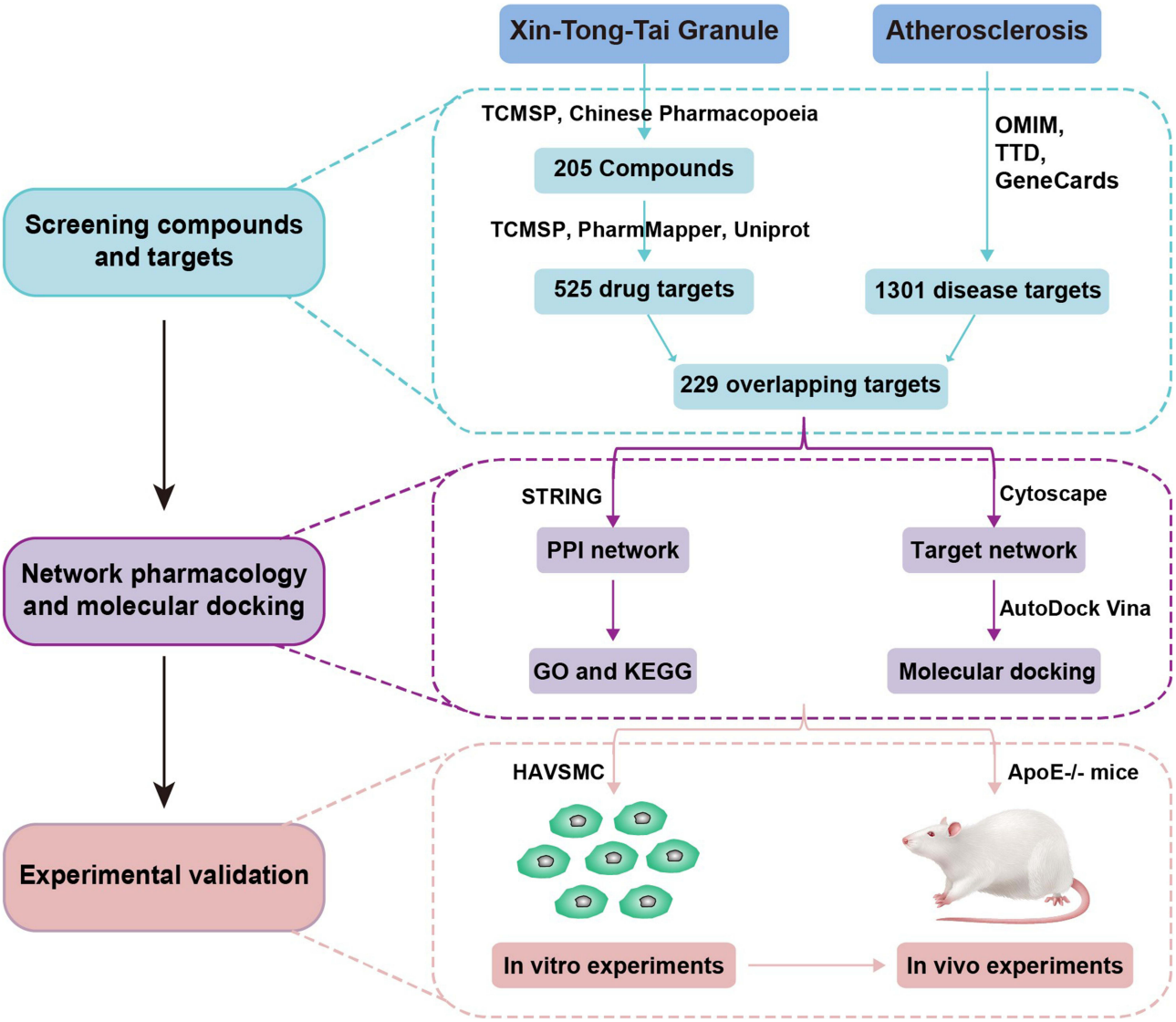

related deaths globally.[2,3] Given its extensive prevalence and mortality, AS has become a focal point of medical research globally. The pathogenesis of AS involves a variety of factors, including inflammation, lipid accumulation, endothelial damage, and the participation of macrophages, endothelial cells (ECs), and smooth muscle cells (SMCs).[4] Present therapeutic approaches, notably statins and other Western medicines, do not fully alleviate AS and are frequently associated with adverse effects that may restrict their application,[5,6] underscoring the pressing need for innovative treatments to tackle this severe condition.

The unique strength of Chinese medicine (CM) in treating various diseases lies in its ability to regulate the disequilibrium within the body and modulate the overarching disease network through a combination of diverse chemical components. Increasingly recognized for its role in managing AS, CM offers benefits such as safety, efficacy, and minimal side effects, making it a valuable alternative to conventional therapies.[7] CM practitioners often attribute the pathogenesis of AS to qi stagnation and blood stasis, which bears some resemblance to the modern medical understanding of impaired blood circulation and endothelial damage. Xin-Tong-Tai Granule (XTTG) is a CM formulation, similar in composition to

Guanxin Pill as listed in the "Volume II of Drug Standards of the Ministry of Public Health of the People's Republic of China —Chinese Medicine Prescription Preparations". It comprises nine herbal components, including Salviae Miltiorrhizae Radix et Rhizoma (Danshen, DS), Chuanxiong Rhizoma (Chuanxiong, CX), Crataegi Fructus (Shanzha, SZ), Notoginseng Radix et Rhizoma (Sanqi, SQ), Aucklandiae Radix (Muxiang, MX), Curcumae Radix (Yujin, YJ), Puerariae Lobatae Radix (Gegen, GG), Aurantii Fructus (Zhiqiao, ZQ), and Glycyrrhizae Radix et Rhizoma (Gancao, GC), that demonstrate properties of enhancing blood flow, eliminating stagnation, balancing qi, and alleviating pain. Studies have shown that XTTG not only significantly mitigates AS symptoms but also regulates blood lipid levels in apolipoprotein E gene knockout ($ApoE^{-/-}$) mice fed a high-fat diet (HFD) and represses the proliferation of human aortic vascular smooth muscle cells (HAVSMCs) induced by oxidized low-density lipoprotein (ox-LDL).[8] Despite these promising results, further research is required to elucidate the precise mechanisms and targets of XTTG in the treatment of AS.

With advancements in network technology and bioinformatics, network pharmacology and molecular docking have emerged as powerful tools to decipher the intricate relationships between CM formulations and diseases. In this study, we utilized network pharmacology and molecular docking to construct an "active compounds-targets-disease" network for XTTG. We then corroborated these findings with both in vitro and in vivo experiments to validate the mechanisms involved, thereby enhancing our understanding of XTTG's therapeutic effects on AS. This integrated approach aims to further capitalize on the benefits of XTTG in treating AS.

Materials and Methods

Materials and Reagents

XTTG: DS 15 g (#1080473), CX 10 g (#1043403), GG 10 g (# 1035903), SQ 3 g (#1052023), YJ 10 g (#1090273), SZ 15 g (#1052373), MX 10 g (#1033923), ZQ 10 g (#1050923), GC 5 g (#1041173), all of these were bought from Guangdong EFONG Pharmaceutical Co., Ltd. (Foshan, China); In our previous report, ultra-performance liquid chromatography-quadrupole-time-of-flight mass spectrometry (UPLC-Q-TOF-MS/MS, Agilent Technologies, Santa Clara, CA, USA) analysis has identified several active components in XTTG, including Puerarin, Neohesperidin, Notoginsenoside r1, Salvianolic acid b, Cryptotanshinone, and Tanshinone IIA (Figure S1 and Table S1).[7] Ammonium pyrrolidithiocarbamate (PDTC) (Cat#S1808) from Beyotime Biotechnology (Shanghai, China); Fetal bovine serum (FBS) (Cat#164210-50), 0.25% trypsin-EDTA solution (Cat#PB180226), and high-glucose Dulbecco minimum essential medium (DMEM) (Cat#150210) from Procell Life Science & Technology Co., Ltd. (Wuhan, China). Ox-LDL (Cat#YB-002-2mg) was sourced from Yiyuan Biotechnology (Guangzhou, China); Cell Counting Kit-8 (CCK-8) (Cat#E-CK-A362) from Elabscience Biotechnology Co., Ltd. (Wuhan, China); Oil Red O (ORO) stain kit (Cat#G1261) from Beijing Solarbio Science & Technology Co., Ltd. (Beijing, China). Enzyme-linked immunosorbent (ELISA) kits for mouse interleukin-6 (IL-6) (Cat#CSB-E04639m) and tumor necrosis factor-α (TNF-α) (Cat#CSB-E04741m) were acquired from Cusabio Biotech (Wuhan, China); Human IL-6 (Cat#MM-0049H1) and human TNF-α (Cat#MM-0122H1) ELISA kits from Jiangsu Meimian Industrial Co., Ltd (Yancheng, China). Assay kits for triglyceride (TG) (Cat#A110-1-1), total cholesterol (TC) (Cat#A111-1-1), high-density lipoprotein cholesterol (HDL-C) (Cat#A112-1-1), and low-density lipoprotein cholesterol (LDL-C) (Cat#A113-1-1) were obtained from Jiancheng Institute of Biotechnology (Nanjing, China). Radio immunoprecipitation assay (RIPA) lysis buffer (Cat#AWB0136), a protease inhibitor (Cat#AWH0645), a phosphatase inhibitor (Cat#AWH0650), a loading buffer (Cat#AWB0055), bicinchoninic acid (BCA) protein assay kit (Cat#HG-WDP0003a), and enhanced chemiluminescence (ECL) chemiluminescence reagent (Cat#AWB0005) were supplied by Abiowell Biotechnology Co., Ltd. (Changsha, China). Antibodies used included: nuclear factor kappa-B (NF-κB) p65 (Cat#10745-1-AP), LC3 (Cat#14600-1-AP), glyceraldehyde 3-phosphate dehydrogenase (GAPDH, Cat#10494-1-AP), β-actin (Cat#66009-1-Ig), and CoraLite488-conjugated Goat Anti-Rabbit IgG (H+L) (Cat#SA00013-2) from proteintech (Wuhan, China); p-NF-κB p65 (Cat#3033) obtained from Cell Signaling Technology (MA, USA); p62 (Cat#ab109012) from Abcam (Cambridge, UK); HRP-conjugated goat anti-mouse (Cat#AWS0001)/rabbit (Cat#AWS0002) secondary antibody from Abiowell Biotechnology Co., Ltd. (Changsha, China).

Network Pharmacology and Molecular Docking

Screening Active Compounds and Targets in XTTG

The active compounds in XTTG were identified with the help of the Traditional Chinese Medicine Systems Pharmacology (TCMSP) database (https://old.tcmsp-e.com/tcmsp.php). Compounds with an oral bioavailability of at least 30% and a drug-likeness score of 0.18 or higher were considered potentially active. Targets of these compounds were retrieved from both TCMSP and PharmMapper (http://www.lilab-ecust.cn/pharmmapper/), and their identities were verified and standardized utilizing the UniProt database (https://www.uniprot.org).

Screening as-Related Targets

The search for AS-related targets involved querying the terms "atherosclerosis" and "atheromatosis" in databases such as Online Mendelian Inheritance in Man (OMIM, https://www.omim.org), Therapeutic Target Database (TTD, http://db.idrblab.net/ttd), and GeneCards (https://www.genecards.org). A Venn diagram was utilized to illustrate the overlap between the targets of active compounds in XTTG and known disease targets.

Construction of "Drugs-Active Components-Targets-Disease" Network

The intersecting targets were imported into the STRING database (http://string-db.org/) to construct a Protein-Protein Interaction (PPI) network, specifying "Homo sapiens" as the species. The resulting network was visualized using Cytoscape 3.9.0 software. Network parameters such as degree (D), closeness centrality (CCT), and betweenness centrality (BC) were analyzed using the CytoNCA plugin. The median values of these parameters were used to refine and highlight the main active components and key targets of XTTG in the treatment of AS.

Bioinformatics Analysis

Gene Ontology (GO) and Kyoto Encyclopedia of Genes and Genomes (KEGG) enrichment analyses were conducted via the STRING database to explore the potential pathways by which XTTG treats AS. Biological processes (BP), molecular functions (MF), cellular components (CC), and KEGG pathways pertinent to the development of AS were selected with a significance level set at $P \leq 0.05$. The results from the GO and KEGG analyses were then visualized as bubble charts on the bioinformatics platform (http://www.bioinformatics.com.cn/).

Molecular Docking

Molecular docking was implemented utilizing the main active compounds of XTTG as ligands. The structures of ligands and proteins were sourced from the ZINC database (https://zinc.docking.org/) and the Protein Data Bank (PDB, https://www.rcsb.org/), respectively. AutoDock Vina 1.1.2 and Chimera 1.16 were utilized for the docking process. The interactions with the highest binding energies between the key targets and the main active components were subsequently visualized to identify the most effective interactions.

Preparation and Preservation of Medicated Serum

Six healthy adult male Sprague-Dawley rats (No. 430727221100544363, weighing 220–240 g) were acquired from Hunan Slake Jingda Experimental Animal Co., Ltd (Hunan, China; License No. SCXK (Xiang) 2019–0004). The rats were housed at the Experimental Animal Center of Hunan University of Chinese Medicine (HNUCM) under controlled conditions (23±2) °C temperature and (56±4) % humidity (eat and drink freely). After a five-day acclimatization period, the rats were administered XTTG at a dose of 4 g/kg/day by oral gavage for seven days. Serum was subsequently collected from these rats and stored in a low-temperature refrigerator (902GP, Thermo Fisher Instrument Co., Ltd, Suzhou, China).

Cell Culture and Handling

HAVSMCs (Procell Life Science&Technology Co., Ltd, Wuhan, China) were cultured in high-glucose DMEM supplemented with 10% FBS and 1% (volume ratio, v/v) penicillin/streptomycin. Cultures were maintained in a 5% CO_2 incubator. Upon reaching 70–80% confluence, the cells were organized into four groups: control (representing blank control), model, XTTG, and PDTC. All groups except the control were exposed to 100 mg/L ox-LDL for 24 h to induce

atherosclerotic conditions. Following this, the medium was replaced in all groups. Treatments for the subsequent 24 h included 10% XTTG-medicated serum for the XTTG group and 100 μmol/L PDTC for the PDTC group, with the model group receiving no further treatment.

Cell Viability Analysis

Cells were seeded in a 96-well plate (2×10^4 cells/mL), with 100 μL of cell suspension per well. Following the respective treatments, each well received 10 μL of CCK-8 reagent. Cell viability was then tested by measuring the optical density (OD) at 450 nm with a Varioskan LUX Microplate Reader (Thermo Fisher Scientific, Waltham, MA, USA).

Animals and Treatment

The Animal Research Ethics Board of HNUCM approved the experiment (Permission Number: LL2021110802). All animal procedures were strictly adhered to the guidelines set by the National Institute of Health's Guide for the Care and Use of Laboratory Animals. Twenty-five specific pathogen free (SPF)-grade healthy male ApoE$^{-/-}$ mice (No. 110322221100858112) and ten SPF-grade healthy male C57BL/6J wild mice (No. 110322221101117945) (aged six to eight weeks and weighing approximately 20±2 g) were obtained from Beijing HFK Bioscience Co., Ltd (Beijing, China; License No. SCXK (Jing) 2019–0008). The mice were housed at the Experimental Animal Center of HNUCM, maintained at (23±2) °C and a humidity of (56±4) % (eat and drink freely). Following five days of acclimatization, the ApoE$^{-/-}$ mice were placed on an HFD consisting of 10% egg yolk powder, 10% lard oil, 1% cholesterol, 0.2% bile salts, and 77.8% base feed for 12 weeks to induce AS. Successful model development was confirmed by the presence of typical atherosclerotic plaques in the aorta via hematoxylin-eosin (HE) staining. Subsequently, the successfully modeled ApoE$^{-/-}$ mice were randomized into a model group, an XTTG group (treated with 6 g/kg XTTG via gavage), and a PDTC group (treated with 20 mg/kg PDTC via gavage). The C57BL/6J wild mice received a standard diet and served as the normal group. Mice in both the normal and model groups were administered an equivalent volume of saline. Treatments were administered daily for eight weeks.

Determination of Mouse Serum Lipid Concentration

Following the experimental period, blood was harvested from the mice and centrifuged at 3500 rpm for 10 min. The serum levels of TG, TC, LDL-C, and HDL-C were quantitatively assessed utilizing a Microplate Reader.

HE Staining

Mouse aortic tissues were preserved in 4% paraformaldehyde, then paraffin-embedded and sectioned into 5-μm slices. These sections underwent deparaffinization in xylene and were rehydrated progressively through an ethanol gradient before being stained with HE. Subsequently, the sections were mounted for examination under a Leica DMI8 microscope (Leica Microsystems, Wetzlar, Germany), with image analysis conducted utilizing Image-Pro Plus 6.0 software.

ORO Staining

Cells were seeded in a 96-well plate (5×10^4 cells/mL), each well containing 500 μL of the cell suspension. Simultaneously, mouse aortic tissues were preserved with 4% paraformaldehyde, dehydrated in a sucrose solution, and prepared for cryosectioning. The resulting cryosections, along with the treated cells, were stained with ORO and analyzed under a microscope, with Image-Pro Plus 6.0 software utilized for image analysis.

ELISA Assay

Supernatants from cultured HAVSMCs and serum from the experimental mice were harvested. The concentrations of TNF-α and IL-6 were tested utilizing specific ELISA kits.

Immunofluorescence Staining

Cells were cultured in 6-well plates (2×10^5 cells/mL), with 1 mL of cell suspension per well. Post-treatment, cells were fixed and permeabilized with 0.3% Triton X-100, blocked with 5% bovine serum albumin (BSA), and incubated

overnight at 4°C with primary antibodies against LC3 and p62 (both at a dilution of 1:100), followed by a secondary antibody treatment (dilution 1:200) for 1 h at ambient temperature in a dark environment. 4',6-Diamidino-2-phenylindole (DAPI, Wellbio, Shanghai, China) was applied for nuclear staining. Visualization was carried out using a Leica DMI8 fluorescence microscope.

Western Blot

Total protein from cells and mouse aortic tissue was extracted using RIPA lysis buffer, with concentrations determined by BCA assay. Proteins were electrophoresed via sodium dodecyl sulfate-polyacrylamide gel electrophoresis (SDS-PAGE) and transferred onto polyvinylidene fluoride (PVDF) membranes. These were blocked with 5% skim milk for 1 h, followed by overnight incubation at 4°C with primary antibodies targeting phosphorylated NF-κB p65 (p-NF-κB p65), NF-κB p65 (both 1:1000), GAPDH (1:5000), LC3 (1:1000), p62 (1:10,000), and β-actin (1:5000). Corresponding secondary antibodies (1:6000) were applied at ambient temperature for 1 h, with band detection using ECL chemiluminescence. Band intensity was analyzed utilizing a Bio-rad Molecular Imager® ChemiDoc™ XRS+ Imaging System with Quantity-One software (Bio-Rad Laboratories, Hercules, CA, USA).

Immunohistochemistry

Mouse aortic tissues were paraffin-embedded, sectioned, and placed in citrate buffer (pH 6.0). Sections were treated with 1% periodic acid for 10 min at ambient temperature, then incubated overnight at 4°C with a primary antibody against NF-κB p65 (1:100), followed by an hour-long incubation with a secondary antibody at ambient temperature. Staining development was performed utilizing 3,3'-Diaminobenzidine (DAB) chromogen and counterstained with hematoxylin. Examination and analysis were done employing a Leica DMI8 microscope and Image-Pro Plus 6.0 software for OD measurements.

Statistical Analysis

Data were analyzed employing SPSS version 27.0, expressed as mean ± standard deviation. Group differences were evaluated employing one-way analysis of variance (ANOVA), with least significant difference (LSD) tests applied for direct comparisons between two groups. Non-parametric tests were utilized as necessary. *P*-value <0.05 described statistically significant.

Results

Screening of Core Components and Targets for XTTG Treatment of as

Initial screening identified 1185 compounds in the XTTG. Distribution of these compounds across the herbal components included 202 from DS, 189 from CX, 32 from SZ, 119 from SQ, 106 from MX, 222 from YJ, 18 from GG, 17 from ZQ, and 280 from GC. Applying thresholds for OB ≥ 30% and DL ≥ 0.18, a total of 208 active compounds were selected. Specifically, these included 65 compounds from DS, 7 from CX, 6 from SZ, 8 from SQ, 6 from MX, 15 from YJ, 4 from GG, 5 from ZQ, and 92 from GC. An additional 11 compounds were included from the 2020 edition of the Chinese Pharmacopoeia and literature, with 1, 1, 1, 3, 2, and 3 compounds respectively sourced from DS, CX, SZ, SQ, MX, and YJ. After eliminating duplicates, 205 unique active compounds remained. Targets associated with these active compounds were identified using the TCMSP and PharmMapper databases. In total, 525 unique targets for XTTG were identified. Of these, 229 targets overlapped between the active compounds and known disease-associated targets, as depicted in Figure 1A and Table S2.

"Drugs-Active Components-Targets-Disease" Network Construction

A confidence level of 0.95 was set for the 229 intersecting targets identified in the STRING database to ensure robust PPI within the network (Figure 1B). The "Drugs-Active Components-Targets-Disease" network was subsequently constructed using Cytoscape 3.9.0 software, comprising 738 nodes and 4593 edges (Figure 1C). Analysis of the topological features, including D, CCT, and BC, highlighted the top 14 targets: Jun proto-oncogene (JUN), Caspase 3 (CASP3), TNF,

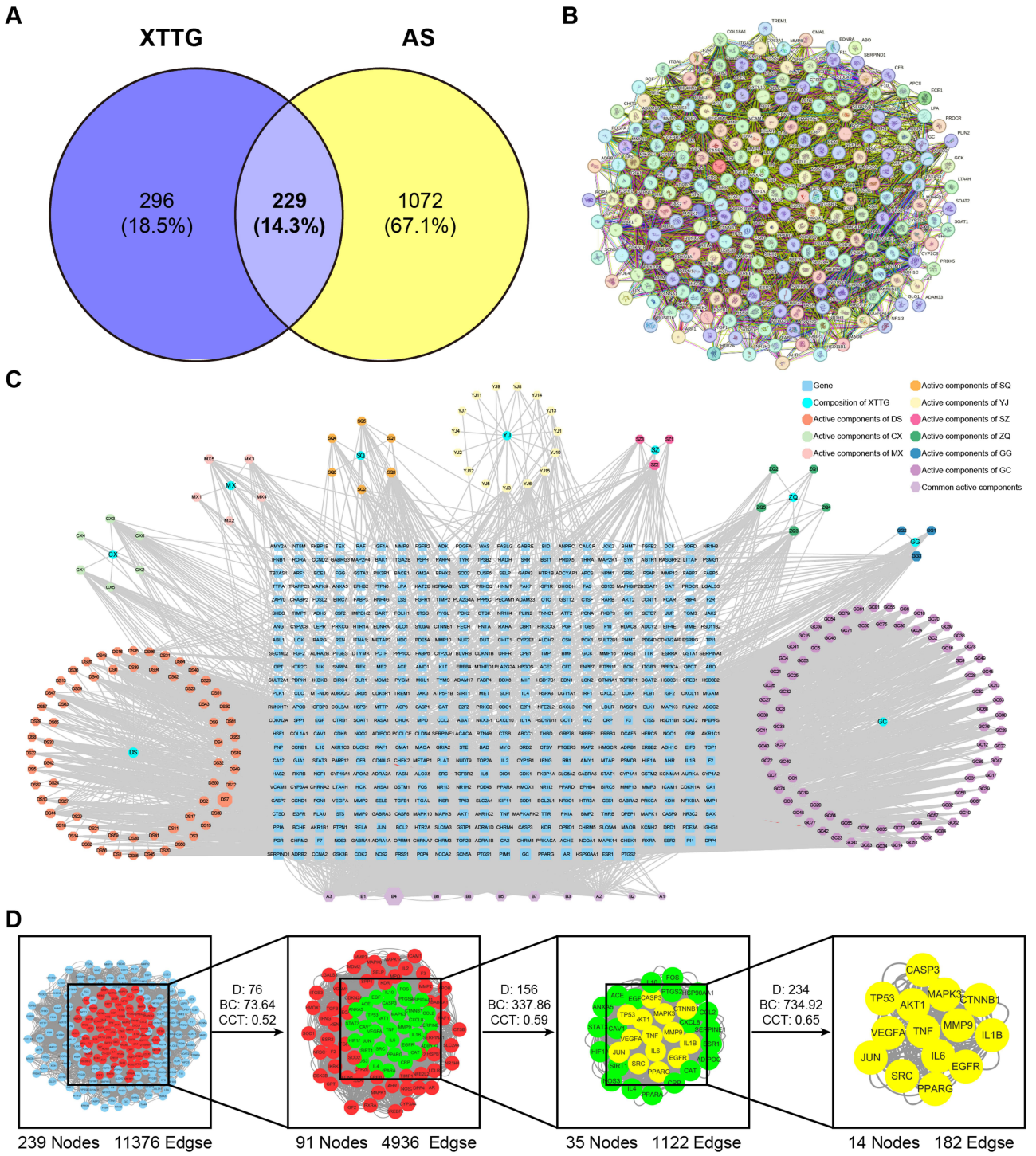

Figure 1 Screening of potential core targets for XTTG treatment of AS. (**A**) Venn diagram of XTTG and AS. (**B**) PPI network diagram of intersection targets of XTTG and AS. (**C**) "XTTG-Active Components-Targets-AS" network. The square represents the gene; the Circular represents the composition of XTTG; the Octagonal represents active components. The size and transparency of each node are proportional to the target degree in the network. (**D**) Screening process of key targets of XTTG in the treatment of AS.

SRC proto-oncogene (SRC), Matrix metalloproteinase-9 (MMP9), IL-6, Epidermal growth factor receptor (EGFR), AKT serine/threonine kinase 1 (AKT1), Vascular endothelial growth factor A (VEGFA), IL-1β, Tumor protein P53 (TP53), Mitogen-activated protein kinase 3 (MAPK3), Peroxisome proliferator-activated receptor gamma (PPARG), and Catenin beta 1 (CTNNB1) (Figure 1D). Among these, seven key targets—TNF, MAPK3, AKT1, IL-6, SRC, IL-1β, and CTNNB1

—were involved in more than 10 pathways each, underscoring their critical roles in the treatment of AS. TNF-α is a pivotal mediator of the inflammatory response, promoting various inflammatory processes linked to AS.[9] MAPK3 (ERK1), a member of the mitogen-activated protein kinase family, modulates the inflammatory response in macrophages, impacting AS plaque formation.[10] AKT1 is essential for endothelial cell function and maintaining vascular integrity.[11] IL-6 influences thrombosis and aneurysm formation associated with AS.[12] SRC affects the senescence of vascular smooth muscle cells (VSMCs) through mechanisms involving cytokine-induced aging, oxidative stress, and vascular remodeling.[13] IL-1β is involved in the activation pathways downstream of the IL-6 receptor, with its cleavage and secretion contributing to plaque deposition in AS.[14] CTNNB1 (rs2953) shows significant correlations with various factors, including lipid levels and inflammatory responses involving eosinophils.[15,16]

Bioinformatics Analysis

The 229 intersecting targets identified were subjected to GO and KEGG pathway enrichment analysis. In the GO analysis, these targets were implicated in 2168 BP primarily involved in Regulation of immune system process, Inflammatory response, Regulation of MAPK cascade, Regulation of smooth muscle cell proliferation, Regulation of lipid metabolic process, Response to oxidative stress, Blood circulation, Regulation of epithelial cell proliferation, Response to growth factor, Regulation of endothelial cell proliferation, Blood vessel development, Regulation of cytokine production, Steroid metabolic process, Regulation of cell adhesion, Regulation of cell activation, Heart development, Regulation of blood pressure, Regulation of I-kappaB kinase/NF-kappaB signaling, Cholesterol metabolic process, and Regulation of autophagy (Figure 2A and Table S3). For MF, 162 categories were enriched, highlighting roles Protein binding, Signaling receptor binding, Enzyme binding, Ion binding, Lipid binding, Cytokine receptor binding, Steroid binding, Receptor ligand activity, Catalytic activity, Peptidase activity, Small molecule binding, Growth factor activity, Antioxidant activity, MAP kinase activity, NF-kappaB binding, Sterol binding, Cholesterol binding, Tumor necrosis factor receptor binding, IkappaB kinase activity, and Arachidonic acid epoxygenase activity (Figure 2B and Table S4). The targets of the 102 enriched CC were mainly developed in Extracellular space, Extracellular region, Vesicle, Membrane raft, Endomembrane system, Cell surface, Cytoplasmic vesicle, Secretory granule, Extracellular exosome, Cell periphery, Caveola, Vesicle lumen, External side of plasma membrane, Intracellular organelle lumen, Side of membrane, Receptor complex, Cytoplasmic vesicle lumen, Intracellular membrane-bounded organelle, Secretory granule lumen, and Cytoplasm (Figure 2C and Table S5). KEGG pathway analysis identified 202 pathways significantly associated with the common targets between XTTG and AS. Critical pathways include those related to Fluid shear stress and AS, IL-17 signaling pathway, TNF signaling pathway, MAPK signaling pathway, Phosphoinositide 3-kinase (PI3K)-AKT signaling pathway, Forkhead box O (FoxO) signaling pathway, Relaxin signaling pathway, Hypoxia-inducible factor 1 (HIF-1) signaling pathway, Toll-like receptor signaling pathway, Adipocytokine signaling pathway, Chemokine signaling pathway, Cyclic adenosine monophosphate (cAMP) signaling pathway, Vascular endothelial growth factor (VEGF) signaling pathway, NF-kappa B signaling pathway, Antifolate resistance, AMP-activated protein kinase (AMPK) signaling pathway, Renin-angiotensin system, Autophagy, Cholesterol metabolism, and Vascular smooth muscle contraction (Figure 2D and Table S6). Notably, both the GO and KEGG analyses underscore the importance of the NF-kappa B signaling pathway, which is crucial in the inflammatory response and autophagy during AS progression.[17] Activation of the NF-kappa B pathway induces the expression of multiple inflammatory mediators, such as TNF-α and IL-6, which contribute to the development of AS.[18] Conversely, it also influences autophagic processes,[19] underlining its dual role in promoting and mitigating disease processes (Figure 2E). Overall, the therapeutic mechanism of XTTG in treating AS may involve modulation of key signaling pathways that regulate inflammation, autophagy, and endothelial function, offering a comprehensive approach to managing this complex disease.

Molecular Docking Validation

The top 12 active components identified in XTTG included cryptotanshinone, salvilenone I, ferulic acid, beta-sitosterol, naringenin, isorhamnetin, kaempferol, quercetin, hesperetin, formononetin, glycyrin, and licoagrocarpin (Figure 3A). Previous research on RAW264.7 mouse macrophage cells induced by lipopolysaccharide (LPS) demonstrated that

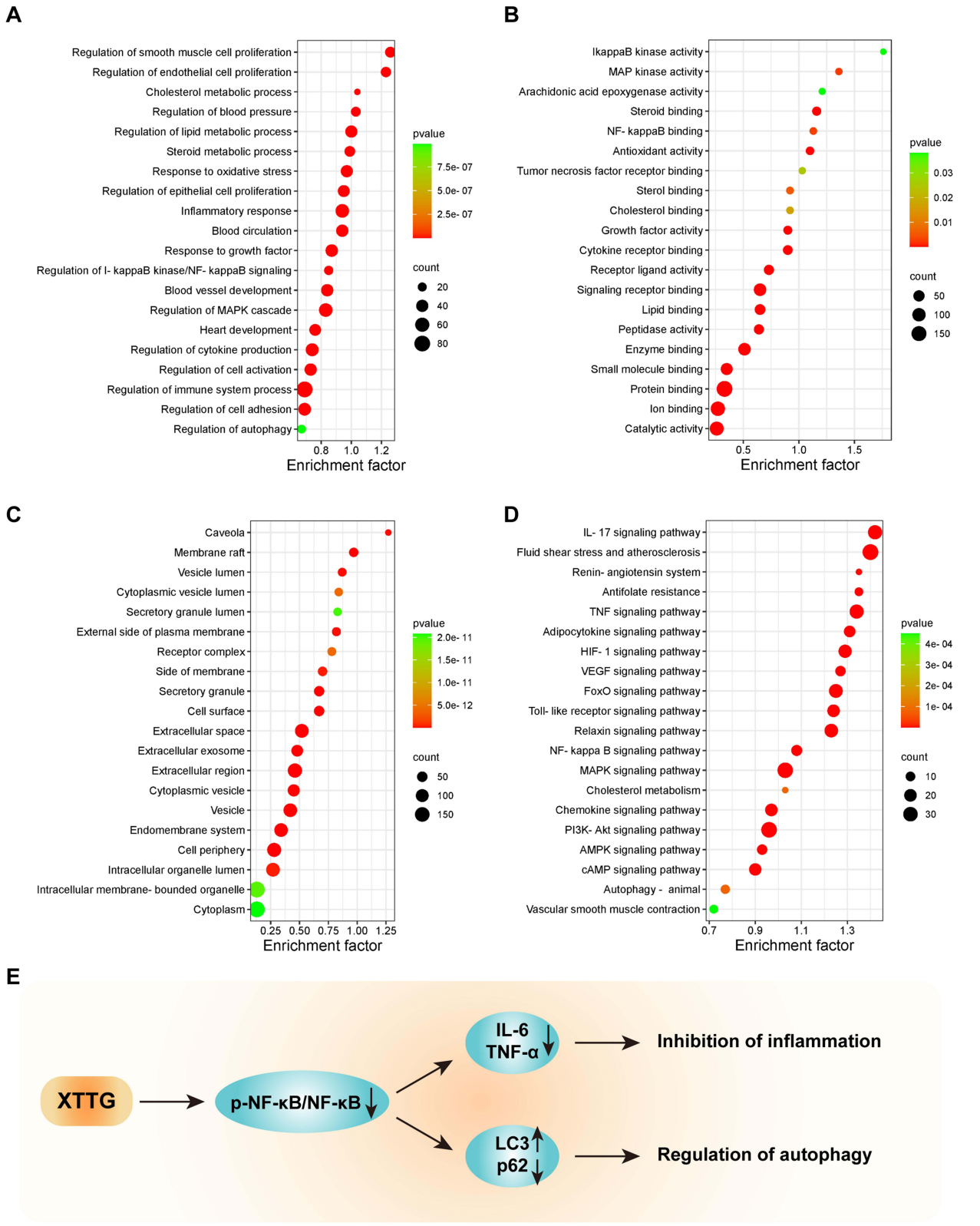

Figure 2 Bioinformatics analysis of intersection targets. (**A-D**) Bubble diagram of BP (**A**), MF (**B**), CC (**C**), and KEGG (**D**) enrichment analysis. (**E**) Prediction mechanism diagram of XTTG treatment for AS.

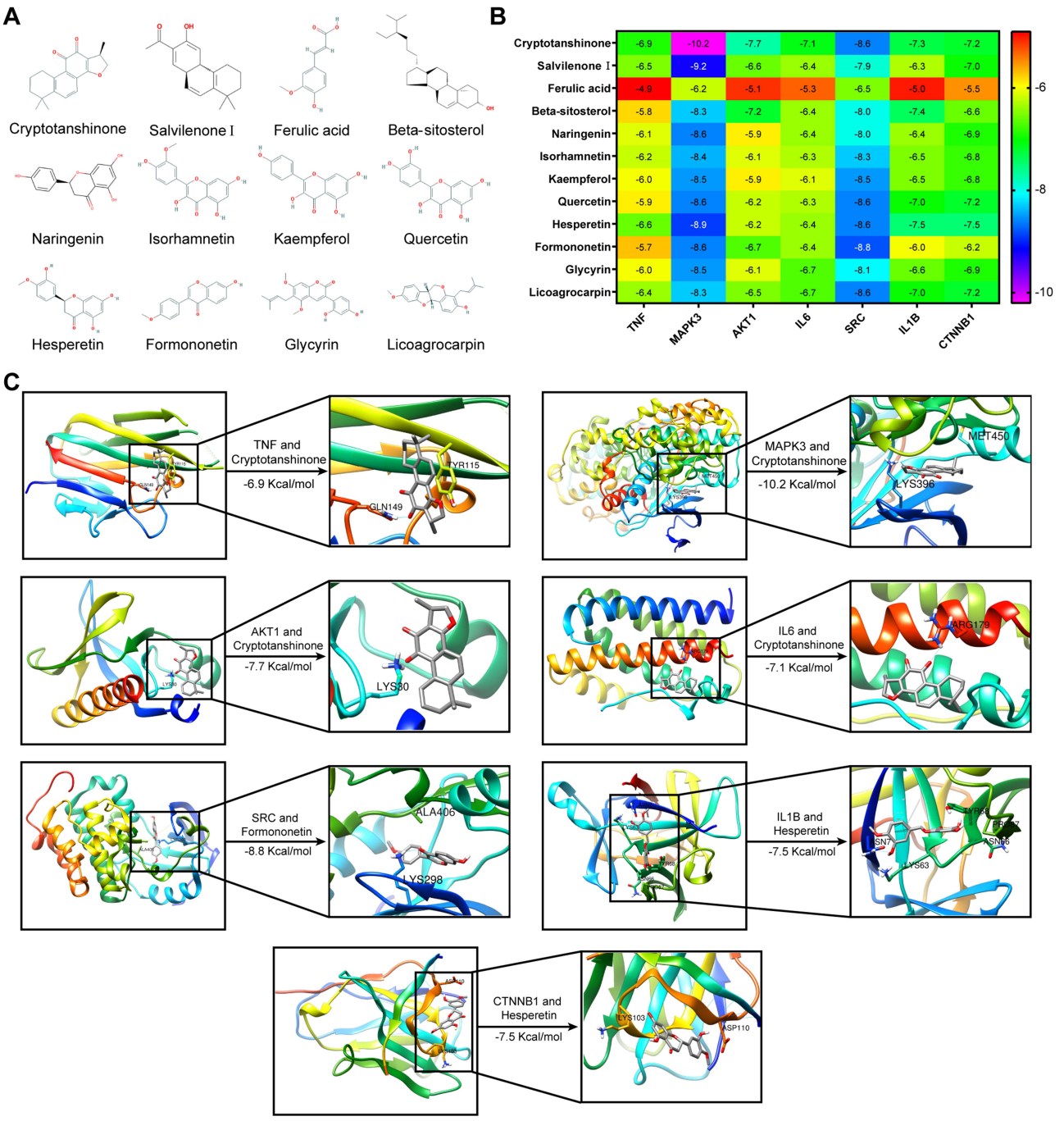

Figure 3 The main active ingredients of XTTG and molecular docking of components and targets. (**A**) Twelve main active components of XTTG. (**B**) Heatmap of molecular docking (Kcal/mol). The purple area corresponds to a lower binding energy and a more stable docking result. (**C**) Analyses of representative targets–compounds docking simulation.

cryptotanshinone significantly reduces inflammatory responses by inhibiting IL-6, TNF-α, Nitric oxide (NO) production, and the expression of NF-κB, PI3K/AKT, and MAPK signaling pathways.[20] Ferulic acid suppresses VSMC proliferation via the NO/p21 signaling pathway.[21] β-sitosterol reduces trimethylamine production and mitigates AS in ApoE$^{-/-}$ mice.[22] Naringenin enhances endothelial function in AS by regulating the AMPK α/Sirtuin 1 (Sirt1) pathway.[23] Isorhamnetin prevents macrophage apoptosis and ameliorates AS by modulating the PI3K/AKT pathway and Heme oxygenase-1 (HO-1) production.[24] Kaempferol offers anti-inflammatory, antioxidant, cardio-protective, and anti-atherosclerotic benefits.[25] Quercetin influences M1/M2 macrophage polarization and the oxidative/antioxidative balance.[26] Formononetin, by

inhibiting SRC phosphorylation, acts as an anti-inflammatory agent.[27] Hesperetin significantly reduces the secretion of TNF-α, IL-6, and IL-1β in LPS-induced RAW 264.7 cells.[28]

Molecular docking was conducted with these 12 primary active compounds and the seven key targets. The docking results revealed varying degrees of binding affinity between the active components and the key targets. All binding energies were robust, with only the interaction between ferulic acid and TNF slightly higher at −4.9 Kcal/mol, while all others were ≤ −5.0 Kcal/mol, indicating excellent affinity (Figure 3B). Cryptotanshinone displayed particularly strong binding to TNF, MAPK3, AKT1, and IL-6 with energies of −6.9, −10.2, −7.7, and −7.1 Kcal/mol, respectively. Formononetin showed the strongest binding to SRC (−8.8 Kcal/mol) and hesperetin to IL-1β and CTNNB1, both at −7.5 Kcal/mol. Notably, according to UPLC-Q-TOF-MS/MS analysis,[8] cryptotanshinone demonstrated superior binding activity to all key targets, underscoring its significance as an active component of XTTG (Figure 3C).

XTTG Repressed the Proliferation and Lipid Droplet Aggregation of HAVSMCs in vitro

Cell proliferation and lipid droplet aggregation in HAVSMCs were enhanced following induction with ox-LDL as compared to the control group. This increase was mitigated after treatment with XTTG or PDTC (an NF-κB inhibitor), as evidenced by CCK-8 and ORO staining results (Figure 4).

XTTG Decreased the Ratio of p-NF-κB p65/NF-κB p65, Inhibited Inflammation and Promoted Autophagy in Ox-LDL-Induced HAVSMCs

Following the insights gained from network pharmacology, this study focused on the role of the NF-κB pathway in regulating inflammation and autophagy in ox-LDL-induced HAVSMCs. ELISA results revealed that ox-LDL induction increased TNF-α and IL-6 levels in HAVSMCs relative to the control group. However, these levels were significantly reduced after treatment with XTTG or PDTC, indicating effective suppression of inflammatory responses (Figure 5A and B). Immunofluorescence staining demonstrated a decrease in LC3 and an increase in p62 protein expression in the model group relative to the control. Contrarily, treatment with XTTG or PDTC led to an increase in LC3 and a decrease in p62 expressions, suggesting enhanced autophagic activity (Figure 5C–F). Western blot analysis further supported these findings, showing an increase in the ratio of p-NF-κB p65 to total NF-κB p65 in the model group compared to the control, indicative of activated NF-κB signaling. This

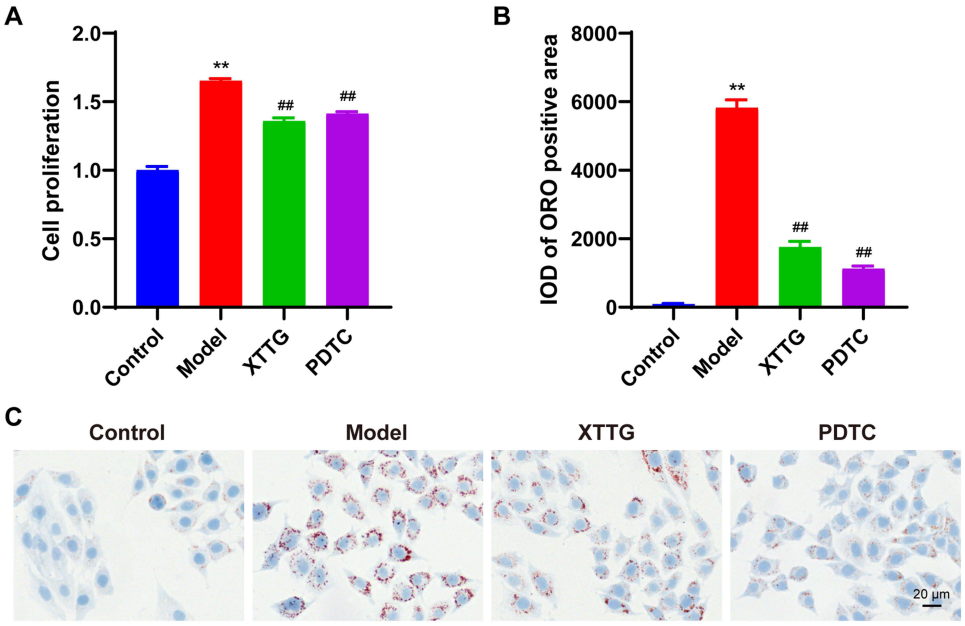

Figure 4 XTTG inhibited the proliferation and lipid droplet aggregation in ox-LDL-induced HAVSMCs. (**A**) Proliferation of HAVSMCs by CCK-8. (**B** and **C**) Representative ORO staining images and semiquantitative analysis of HAVSMCs, magnification 200×. n = 3. $^{**}P < 0.01$ vs control group; $^{\#\#}P < 0.01$ vs model group.

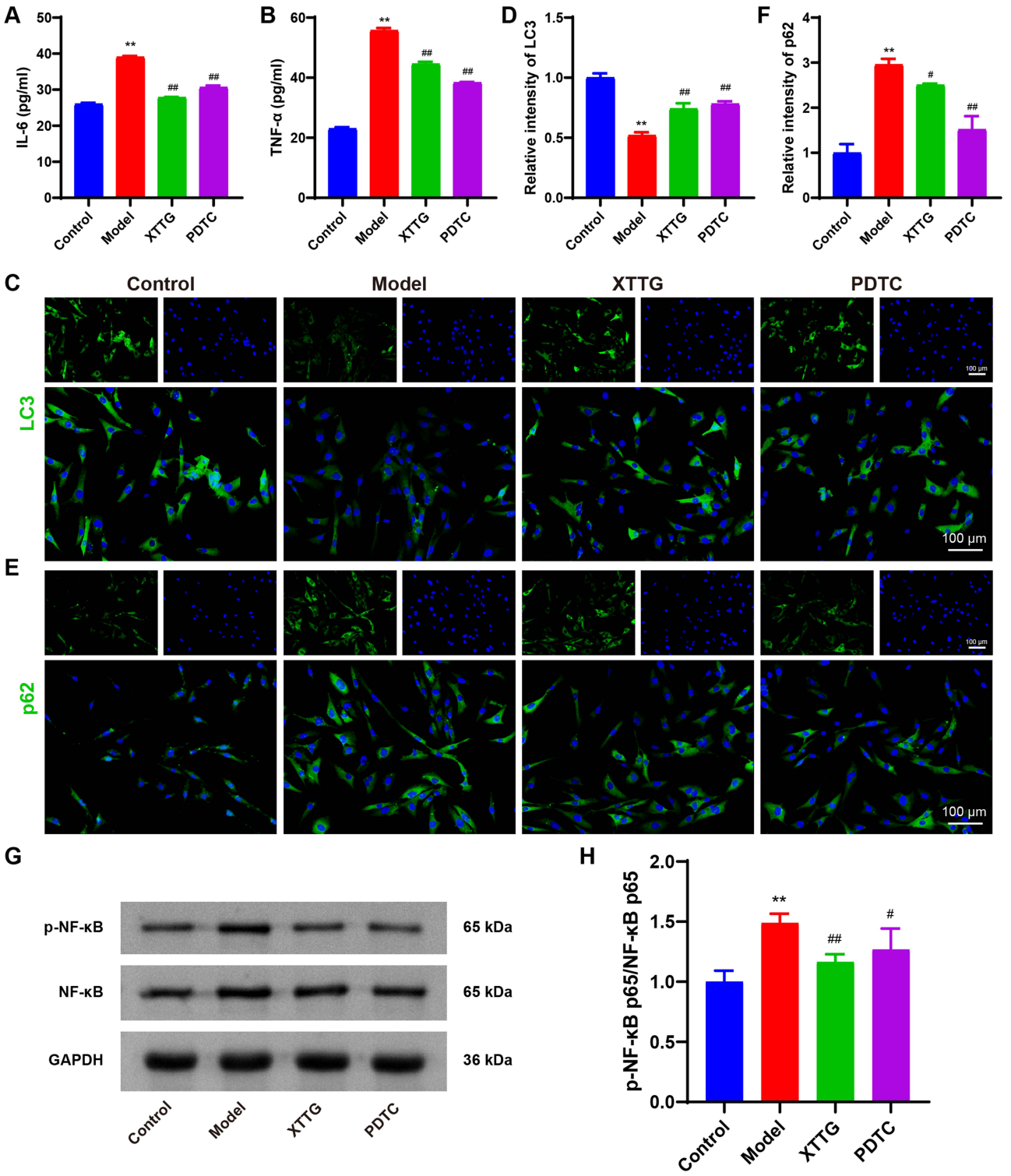

Figure 5 XTTG decreased the ratio of p-NF-κB p65/NF-κB p65, inhibited inflammation and promoted autophagy in ox-LDL-induced HAVSMCs. (**A** and **B**) the levels of TNF-α or IL-6 by ELISA in HAVSMCs. (**C–F**) Representative images and quantitative analysis by immunofluorescence staining of LC3 and p62 protein expression in HAVSMCs. (**G** and **H**) Representative images and quantitative analysis by Western blot of p-NF-κB p65/NF-κB p65 in HAVSMCs. n = 3. $^{**}P < 0.01$ vs control group; $^{\#}P < 0.05$ vs model group; $^{\#\#}P < 0.01$ vs model group.

ratio was notably decreased in the XTTG and PDTC treatment groups, underscoring the potential of XTTG and PDTC to modulate NF-κB activity and thereby attenuate inflammation and promote autophagy in this cellular model of AS (Figure 5G and H).

XTTG Attenuated the Development of HFD-Induced as in ApoE$^{-/-}$ Mice

In our study, the therapeutic effects of XTTG were assessed in ApoE $^{-/-}$ mice fed with HFD. Initially, serum levels of TC, TG, and LDL-C were elevated, while HDL-C levels were reduced in ApoE$^{-/-}$ mice compared to C57BL/6J wild mice on a standard diet. Treatment with XTTG or PDTC effectively decreased serum levels of TC, TG, and LDL-C, and increased HDL-C levels (Figure 6A–D). HE staining revealed a structurally normal aorta with an intact elastic fiber structure and no atherosclerotic plaque formation in the normal group (Figure 6E and F). In contrast, the model group exhibited typical atherosclerotic plaques, elastic fiber disruption, and subendothelial space expansion, which were significantly mitigated by XTTG or PDTC treatment. ORO staining confirmed these observations, showing no aortic intimal thickening or lipid deposits in the normal group, whereas prominent intimal thickening and lipid-rich areas were evident in the model group. XTTG or PDTC treatment reduced aortic intimal thickening and the extent of lipid deposition (Figure 6G and H).

XTTG Inhibited Inflammation, Promoted Autophagy, and Decreased NF-κB p65 Positive Protein Expression in the Aorta of HFD-Induced as in ApoE$^{-/-}$ Mice

In ApoE$^{-/-}$ mice on an HFD, serum levels of TNF-α and IL-6 were increased relative to normal. Administration of XTTG or PDTC significantly lowered these inflammatory markers (Figure 7A and B). Western blot analysis noted that the ratio of LC3 II/LC3 I decreased, and p62 expression increased in the model group relative to the normal group. However, treatment with XTTG or PDTC reversed these trends, increasing the ratio of LC3 II/LC3 I and decreasing p62

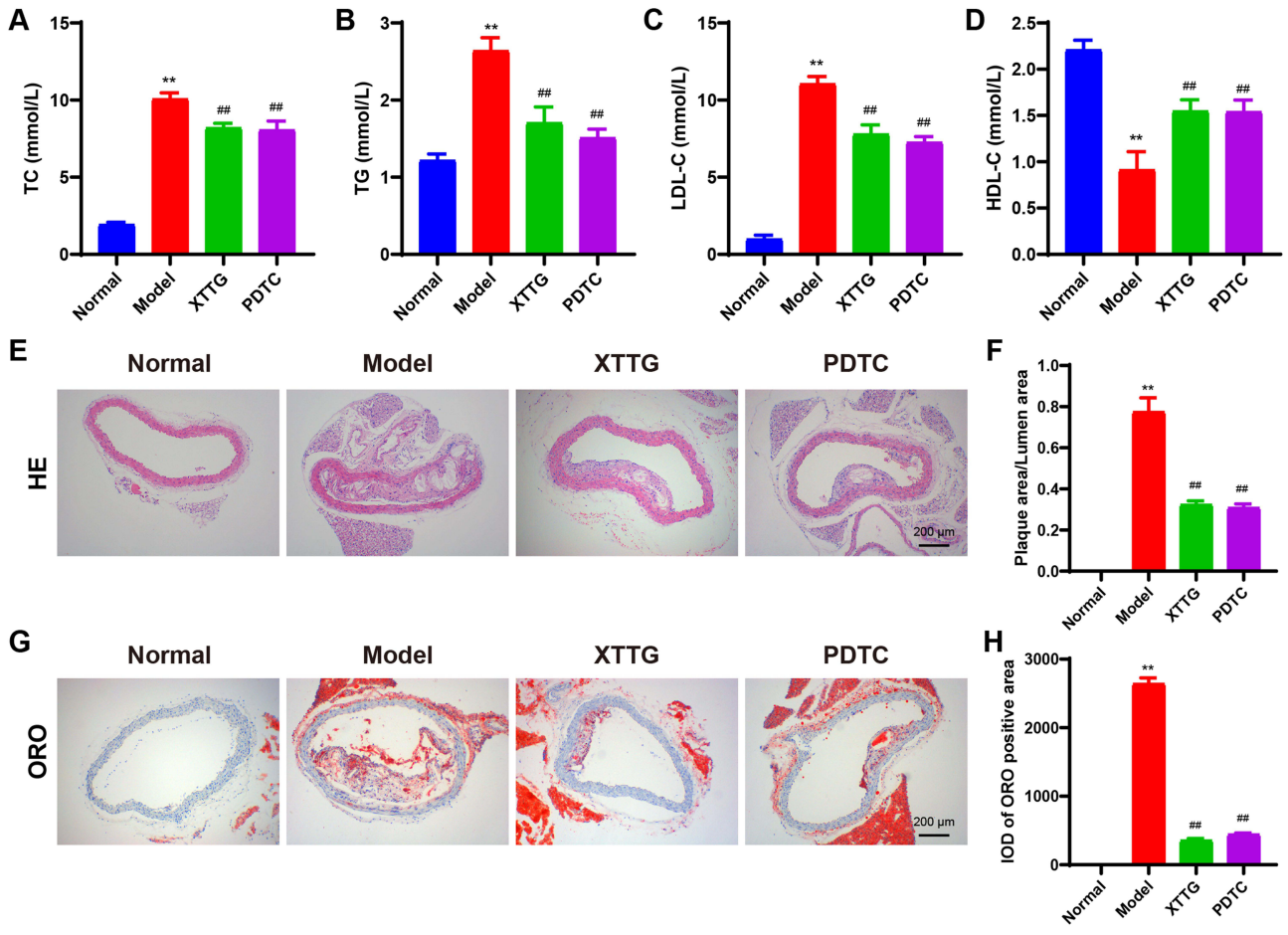

Figure 6 XTTG attenuated the development of HFD-induced atherosclerosis in ApoE$^{-/-}$ mice. (**A-D**) Results of serum TC, TG, LDL-C and HDL-C levels of mice (n = 6). (**E** and **F**) Representative HE staining images and semiquantitative analysis of the aorta in mice, magnification 40× (n = 3). (**G** and **H**) Representative ORO staining images and semiquantitative analysis of the aorta in mice, magnification 40× (n = 3). $^{**}P < 0.01$ vs normal group; $^{\#\#}P < 0.01$ vs model group.

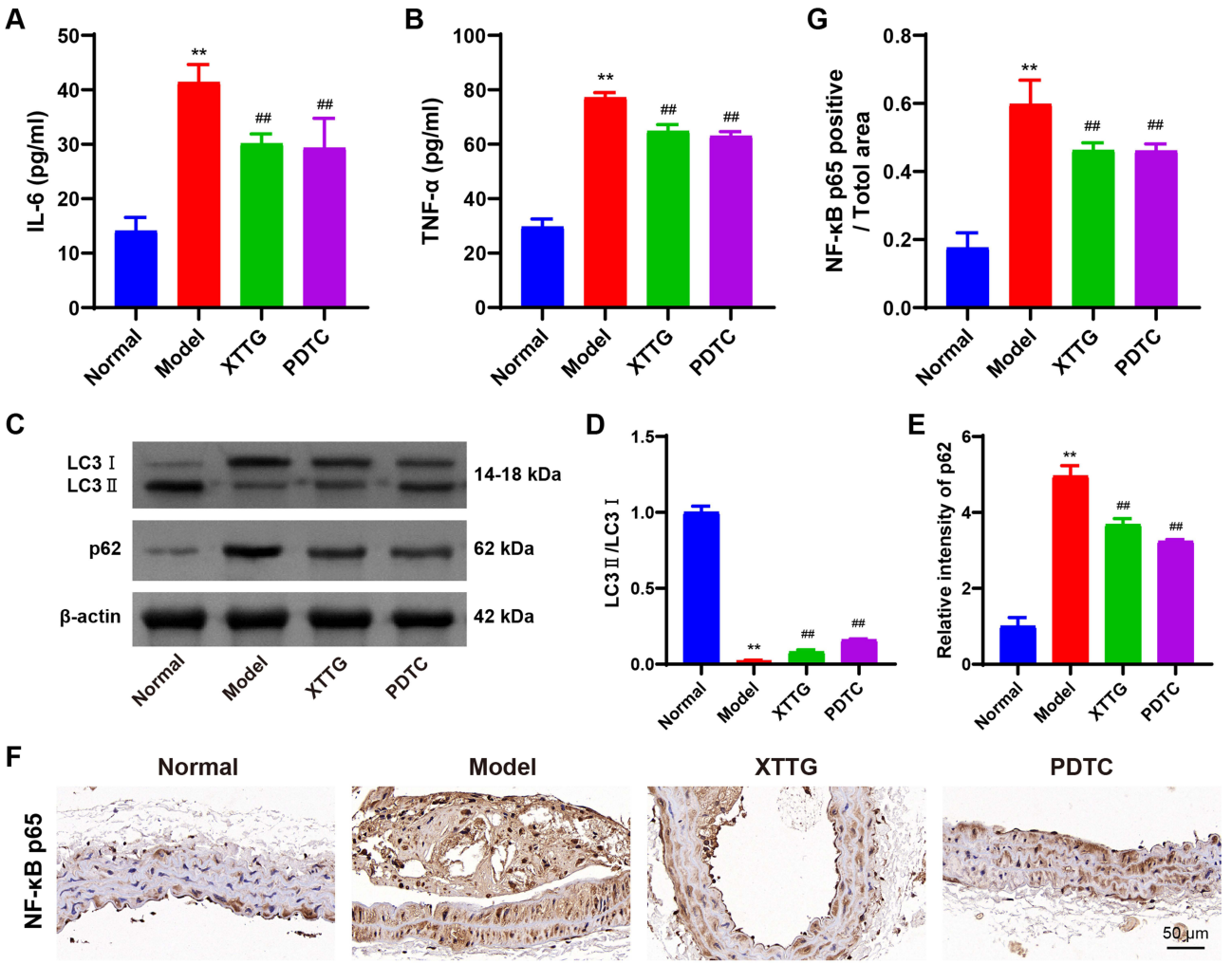

Figure 7 XTTG inhibited inflammation and promoted autophagy, decreased NF-κB p65 positive protein expression in the aorta of ApoE$^{-/-}$ mice with HFD-induced. (**A** and **B**) Results of serum levels of TNF-α and IL-6. (**C–E**) Representative images and quantitative analysis by Western blot of LC3II/LC3I and p62 protein expression in the aorta of mice. (**F** and **G**) Representative images and semiquantitative analysis by immunohistochemistry of NF-κB p65 positive protein expression in aorta of mice. n = 3. $^{**}P < 0.01$ vs normal group; $^{\#\#}P < 0.01$ vs model group.

protein expression, revealing enhanced autophagic activity (Figure 7C–E). Immunohistochemistry analysis further showed that NF-κB p65 positive protein expression was higher in the model group than in the normal group, but was reduced following XTTG or PDTC treatment (Figure 7F and G). These results suggest that XTTG effectively inhibits NF-κB p65 expression, exerting anti-inflammatory effects and promoting autophagy in AS.

Discussion

AS is a multifaceted and progressive disease characterized by lipid accumulation and inflammatory responses.[29] The hallmark of AS is the presence of atherosclerotic plaques,[1] which are characterized by a fibrous cap that covers an internal lipid core rich in lipids, necrotic cells, and an inflammatory milieu. Inflammation not only exacerbates the formation and instability of these plaques but also is pivotal in their rupture, leading to severe cardiovascular events.[2] Concurrently, autophagy, a vital cellular metabolic process, is increasingly recognized for its significant role in the development and stability of atherosclerotic plaques.[30] XTTG, an effective CM compound, has been shown to reduce blood lipid levels and inhibit plaque development in the treatment of AS. However, the underlying mechanisms remain insufficiently understood. In previous studies,[31] we investigated the metabolism and distribution of XTTG in rat serum, confirmed 19 circulating components in vivo, and conducted a network pharmacology analysis of its potential targets. However, we did not conduct validation experiments. In addition, these 19 circulating components do not fully represent

the pharmacological components of XTTG. To further explore the mechanism of action of XTTG in treating AS, we utilized widely recognized databases to screen the drug components and targets of the entire XTTG in this study. Subsequently, we reasonably designed a pathway inhibitor group and conducted both in vivo and in vitro experimental validation using techniques such as immunofluorescence, immunohistochemistry, and Western blot. Through this comprehensive analysis, we aim to elucidate the multifunctional roles of XTTG in modulating lipid profiles, inflammatory responses, and autophagic processes within AS, thereby providing a deeper understanding of its therapeutic potential and molecular basis for AS management.

Initially, we conducted a comprehensive integration of Chinese medicine formulas and disease targets, identifying a total of 229 therapeutic targets for XTTG in the treatment of AS. Notably, TNF, MAPK3, AKT1, IL-6, SRC, IL-1β, and CTNNB1 were recognized as key targets. TNF, IL-6, and IL-1β are prominent inflammatory factors that play critical roles in the inflammatory processes associated with AS.[32] Through topological analysis of the herbs-active compounds-targets-disease network, we identified cryptotanshinone, salvilenone I, ferulic acid, beta-sitosterol, naringenin, isorhamnetin, kaempferol, quercetin, hesperetin, formononetin, glycyrin, and licoagrocarpin as the principal active compounds of XTTG. Molecular docking studies confirmed strong affinities between these major bioactive components and the critical targets. Subsequent GO and KEGG enrichment analyses highlighted significant enrichment in several key domains. Among them, BP were predominantly enriched in inflammatory responses, regulation of I-κB kinase/NF-κB signaling, and autophagy. MF were chiefly associated with NF-κB binding and IκB kinase activity. Key KEGG pathways included the IL-17 signaling pathway, TNF signaling pathway, NF-κB signaling pathway, and autophagy, all of which are crucial in the pathogenesis of AS. Notably, the NF-κB signaling pathway was significantly enriched across GO categories and KEGG pathways, underscoring its critical role in inflammation, oxidative stress, and autophagy—processes pivotal to AS development.[17,33] Previous research has demonstrated that XTTG effectively modulates the NF-κB signaling pathway in HAVSMCs and ApoE$^{-/-}$ mice.[8] This evidence led us to explore whether the NF-κB pathway mediates the anti-inflammatory and autophagy-regulating effects of XTTG. To test this hypothesis, we designed both in vitro and in vivo experiments aimed at confirming the involvement of the NF-κB pathway in the therapeutic actions of XTTG, potentially providing a mechanistic basis for its effects on AS.

Abnormal proliferation of SMCs is a pivotal factor in the development of AS.[34] Commonly, ox-LDL induction is used to simulate AS models in vitro.[35] In this context, we employed an ox-LDL-induced model to examine the effects of XTTG intervention. Our findings revealed that XTTG-medicated serum repressed the proliferation of HAVSMCs and reduced lipid droplet aggregation. Further analyses of inflammatory factors and autophagy markers indicated that XTTG not only reduced levels of TNF-α and IL-6 but also enhanced LC3 protein expression while suppressing p62 protein expression. Notably, similar effects were observed with PDTC (an NF-κB inhibitor) intervention. In vivo experiments further supported these results. Oral administration of XTTG improved blood lipid profiles and alleviated pathological changes in the aortas of ApoE$^{-/-}$ mice fed an HFD. This treatment also decreased serum levels of TNF-α and IL-6, increased the ratio of LC3II/LC3I, reduced p62 protein expression, and downregulated NF-κB p65 positive protein expression. Interestingly, similar trends were noted following the PDTC administration. The NF-κB family, which is pervasive across various animals and cell types, comprises five members: RelA (p65), RelB, c-Rel, NF-κB1 (p50), and NF-κB2 (p52).[36] Upon stimulation, the IKK-α and IKK-β in the IκB kinase (IKK) complex are activated, leading to the release of NF-κB from the cytoplasmic NF-κB/IκBα complex and its subsequent translocation to the nucleus. As a prominent member of this family, NF-κB p65 plays a critical role in inflammatory processes and plaque progression in AS.[37] The activation of NF-κB p65 stimulates the expression of TNF-α and IL-6, which contribute to excessive inflammatory responses.[38] Furthermore, NF-κB p65 is closely associated with the regulation of autophagy. Upon activation, NF-κB p65 influences the expression of autophagy-related proteins, including LC3 and p62, thereby affecting the autophagic degradation process.[39] In summary, our research elucidates that XTTG can effectively regulate NF-κB p65 expression, diminish key inflammatory targets TNF-α and IL-6, and modulate pathways related to inflammation and autophagy, thereby providing comprehensive mechanistic insights into its therapeutic potential for managing AS.

While our research has provided novel insights into the molecular mechanisms underlying the treatment of AS with XTTG, several limitations warrant attention. Firstly, although we demonstrated XTTG's role in regulating inflammation

and autophagy through the inhibition of NF-κB p65 expression, the active components within XTTG responsible for these effects were only predicted and not individually studied. This highlights a gap in our understanding of which specific components contribute to the observed effects. Secondly, our in vitro experiments were primarily focused on the role of HAVSMCs in AS. However, AS pathogenesis involves various cell types, including macrophages and ECs, and the complex interactions between these cells were not fully explored in our study. Future research should aim to develop more sophisticated three-dimensional models that incorporate multiple cell types to better mimic the intricate pathogenesis of AS.

Conclusion

This study elucidated the mechanism of XTTG in treating AS through a combination of network pharmacology and molecular docking, supported by in vitro and in vivo validations. We discovered that XTTG effectively inhibits NF-κB p65 expression, thereby modulating inflammation and autophagy. These findings pave the way for further experimental and clinical investigations, enhancing our understanding of XTTG's therapeutic potential and laying the foundation for future research into its clinical applications and the detailed exploration of its active constituents.

Abbreviations

AKT1, AKT serine/threonine kinase 1; AMPK, AMP-activated protein kinase; ANOVA, Analysis of variance; ApoE$^{-/-}$, Apolipoprotein E gene knockout; AS, Atherosclerosis; BC, Betweenness centrality; BCA, Bicinchoninic acid; BP, biological process; BSA, Bovine serum albumin; cAMP, Cyclic adenosine monophosphate; CASP3, Caspase 3; CC, Cellular component; CCT, Closeness centrality; CCK-8, Cell counting kit-8; CTNNB1, Catenin beta 1; CX, Chuanxiong Rhizoma; D, Degree; DAB, 3,3'-Diaminobenzidine; DAPI, 4',6-Diamidino-2-phenylindole; DL, Drug-likeness; DMEM, Dulbecco minimum essential medium; DS, Salviae Miltiorrhizae Radix Et Rhizoma; ECL, Enhanced chemiluminescence; ECs, Endothelial cells; EGFR, Epidermal growth factor receptor; FBS, Fetal bovine serum; FoxO, Forkhead box O; GAPDH, Glyceraldehyde 3-phosphate dehydrogenase; GC, Glycyrrhizae Radix Et Rhizoma; GG, Puerariae Lobatae Radix; GO, Gene Ontology; HAVSMCs, Human aortic vascular smooth muscle cells; HDL-C, High-density lipoprotein cholesterol; HE, Hematoxylin-eosin; HFD, high-fat diet; HIF-1, Hypoxia-inducible factor 1; HO-1, Heme oxygenase-1; LC3, Microtubule-associated protein light chain 3; IL-6, Interleukin-6; JUN, Jun proto-oncogene; KEGG, Kyoto Encyclopedia of Genes and Genomes; LDL-C, Low-density lipoprotein cholesterol; LSD, Least significant difference; MAPK3, Mitogen-activated protein kinase 3; MF, molecular function; MMP9, Matrix metalloproteinase-9; MX, Aucklandiae Radix; NF-κB, nuclear factor kappa-B; NO, Nitric oxide; OB, Oral bioavailability; OD, Optic density; OMIM, Online Mendelian Inheritance in Man; ORO, Oil red o; Ox-LDL, Oxidized low-density lipoprotein; PDTC, Pyrrolidithiocarbamate; PPARG, Peroxisome proliferator-activated receptor gamma; PI3K, Phosphoinositide 3-kinase; PVDF, Polyvinylidene fluoride; RIPA, Radio immunoprecipitation assay; SMCs, Smooth muscle cells; SDS-PAGE, sodium dodecyl sulfate-polyacrylamide gel electrophoresis; SPF, Specific pathogen free; SQ, Notoginseng Radix Et Rhizoma; Sirt1, Sirtuin 1; SRC, SRC proto-oncogene; SZ, Crataegi Fructus; TC, Total cholesterol; TCMSP, Traditional Chinese Medicine Systems Pharmacology; TG, Triglyceride; TP53, Tumor protein P53; TTD, Therapeutic Target Database; TNF-α, Tumor necrosis factor-α; UPLC-Q-TOF-MS/MS, Ultra-performance liquid chromatography-quadrupole-time-of-flight mass spectrometry; VEGF, Vascular endothelial growth factor; VEGFA, Vascular endothelial growth factor A; XTTG, Xin-Tong-Tai Granule; YJ, Curcumae Radix; ZQ, Aurantii Fructus.

Data Sharing Statement

The original contributions presented in the study are included in the article, further inquiries can be directed to the corresponding author.

Acknowledgments

We sincerely appreciate the efforts of all authors who contributed to this study.

Author Contributions

All authors made a significant contribution to the work reported, whether that is in the conception, study design, execution, acquisition of data, analysis and interpretation, or in all these areas; took part in drafting, revising or critically reviewing the article; gave final approval of the version to be published; have agreed on the journal to which the article has been submitted; and agree to be accountable for all aspects of the work.

Funding

This work was supported by the Key Research Project of the Education Department of Hunan Province (20A384) and the Key project of the First-class Discipline of Chinese medicine of Hunan University of Chinese Medicine (2021ZYX14).

Disclosure

The authors declare that the research was conducted in the absence of any commercial or financial relationships that could be construed as a potential conflict of interest.

References

1. Xu X, Qiu F, Yang M, et al. Unveiling atherosclerotic plaque heterogeneity and SPP1+/VCAN+ macrophage subtype prognostic significance through integrative single-cell and bulk-seq analysis. *J Inflamm Res*. 2024;17:2399–2426. doi:10.2147/jir.s454505
2. Gallucci G, Turazza FM, Inno A, et al. Atherosclerosis and the bidirectional relationship between cancer and cardiovascular disease: from bench to bedside-part 1. *Int J Mol Sci*. 2024;25(8):4232. doi:10.3390/ijms25084232
3. Martelli E, Enea I, Zamboni M, et al. Focus on the most common paucisymptomatic vasculopathic population, from diagnosis to secondary prevention of complications. *Diagnostics*. 2023;13(14):2356–2376. doi:10.3390/diagnostics13142356
4. Zhang L, Wu X, Hong L. Endothelial reprogramming in atherosclerosis. *Bioengineering*. 2024;11(4):325. doi:10.3390/bioengineering11040325
5. Poznyak AV, Bharadwaj D, Prasad G, et al. Renin-angiotensin system in pathogenesis of atherosclerosis and treatment of CVD. *Int J Mol Sci*. 2021;22(13):6702. doi:10.3390/ijms22136702
6. Yu W, Wu W, Zhao D, et al. Idebenone ameliorates statin-induced myotoxicity in atherosclerotic ApoE-/- mice by reducing oxidative stress and improving mitochondrial function. *BBA-Mol Basis Dis*. 2024;1870(5):167157. doi:10.1016/j.bbadis.2024.167157
7. Wang X, Xing X, Huang P, et al. A Chinese classical prescription xuefu zhuyu decoction in the treatment of coronary heart disease: an overview. *Heliyon*. 2024;10(7):e28919. doi:10.1016/j.heliyon.2024.e28919
8. Wei JM, Yuan H, Liu CX, et al. The Chinese medicine Xin-tong-tai granule protects atherosclerosis by regulating oxidative stress through NOX/ROS/NF-κB signal pathway. *Biomed Pharmacother*. 2023;165:115200. doi:10.1016/j.biopha.2023.115200
9. Kim CW, Oh ET, Park HJ. A strategy to prevent atherosclerosis via TNF receptor regulation. *FASEB J*. 2021;35(3):e21391. doi:10.1096/fj.202000764R
10. You D, Qiao Q, Ono K, et al. miR-223-3p inhibits the progression of atherosclerosis via down-regulating the activation of MEK1/ERK1/2 in macrophages. *Aging-US*. 2022;14(4):1865–1878. doi:10.18632/aging.203908
11. Liu T, Liu J, Hao L. Network pharmacological study and molecular docking analysis of qiweitangping in treating diabetic coronary heart disease. *Evid-based compl alt*. 2021;2021:9925556. doi:10.1155/2021/9925556
12. Ridker P, Rane M. Interleukin-6 signaling and anti-interleukin-6 therapeutics in cardiovascular disease. *Circ Res*. 2021;128(11):1728–1746. doi:10.1161/circresaha.121.319077
13. Hu BA, Sai WW, Yuan J, et al. PGF2α-FP receptor ameliorates senescence of VSMCs in vascular remodeling by Src/PAI-1 signal pathway. *Oxid Med Cell Longev*. 2022;2022:2908261. doi:10.1155/2022/2908261
14. Satish M, Agrawal D. Atherothrombosis and the NLRP3 inflammasome - endogenous mechanisms of inhibition. *Transl Res*. 2020;215:75–85. doi:10.1016/j.trsl.2019.08.003
15. Zhao X, Hu S, Yang J, et al. A 3' Untranslated region polymorphism of CTNNB1 (Rs2953) alters miR-3161 binding and affects the risk of ischemic stroke and coronary artery disease in Chinese han population. *Eur Neurol*. 2021;84(2):85–95. doi:10.1159/000514543
16. Gao H, Yu Z, Li Y, et al. miR-100-5p in human umbilical cord mesenchymal stem cell-derived exosomes mediates eosinophilic inflammation to alleviate atherosclerosis via the FZD5/Wnt/β-catenin pathway. *Acta Bioch Bioph Sin*. 2021;53(9):1166–1176. doi:10.1093/abbs/gmab093
17. Meng Q, Pu L, Lu Q, et al. Morin hydrate inhibits atherosclerosis and LPS-induced endothelial cells inflammatory responses by modulating the NFκB signaling-mediated autophagy. *International Immunopharmacology*. 2021;100:108096. doi:10.1016/j.intimp.2021.108096
18. Wang Z, Gao Z, Zheng Y, et al. Melatonin inhibits atherosclerosis progression via galectin-3 downregulation to enhance autophagy and inhibit inflammation. *Journal of Pineal Research*. 2023;74(3):e12855. doi:10.1111/jpi.12855
19. Chen M, Liu S. Atorvastatin reduces calcification in valve interstitial cells via the NF-κB signalling pathway by promoting Atg5-mediated autophagy. *Eur J Histochem*. 2024;68(2):3983. doi:10.4081/ejh.2024.3983
20. Li X, Zheng X, Liu Z, et al. Cryptotanshinone from salvia miltiorrhiza bunge (Danshen) inhibited inflammatory responses via TLR4/MyD88 signaling pathway. *Chin Med*. 2020;15(1):20. doi:10.1186/s13020-020-00303-3
21. Wu X, Hu Z, Zhou J, et al. Ferulic acid alleviates atherosclerotic plaques by inhibiting VSMC proliferation through the NO/p21 signaling pathway. *J Cardiovasc Transl*. 2022;15(4):865–875. doi:10.1007/s12265-021-10196-8
22. Wu W, Liu W, Wang H, et al. β-sitosterol inhibits trimethylamine production by regulating the gut microbiota and attenuates atherosclerosis in ApoE$^{-/-}$ mice. *Front Cardiovasc Med*. 2022;9:986905. doi:10.3389/fcvm.2022.986905
23. Li H, Liu L, Cao Z, et al. Naringenin ameliorates homocysteine induced endothelial damage via the AMPKα/Sirt1 pathway. *J Adv Res*. 2021;34:137–147. doi:10.1016/j.jare.2021.01.009

24. Luo Y, Sun G, Dong X, et al. Isorhamnetin attenuates atherosclerosis by inhibiting macrophage apoptosis via PI3K/AKT activation and HO-1 induction. *PLoS One*. 2015;10(3):e0120259. doi:10.1371/journal.pone.0120259
25. Chen M, Xiao J, El-Seedi HR, et al. Kaempferol and atherosclerosis: from mechanism to medicine. *Crit Rev Food Sci*. 2024;64(8):2157–2175. doi:10.1080/10408398.2022.2121261
26. Tsai CF, Chen GW, Chen YC, et al. Regulatory effects of quercetin on M1/M2 macrophage polarization and oxidative/antioxidative balance. *Nutrients*. 2021;14(1):67. doi:10.3390/nu14010067
27. Xiang K, Shen P, Gao Z, et al. Formononetin protects LPS-induced mastitis through suppressing inflammation and enhancing Blood-milk barrier integrity via AhR-induced Src inactivation. *Front Immunol*. 2022;13:814319. doi:10.3389/fimmu.2022.814319
28. Ren H, Hao J, Liu T, et al. Hesperetin suppresses inflammatory responses in lipopolysaccharide-induced RAW 264.7 cells via the inhibition of NF-κB and activation of Nrf2/HO-1 pathways. *Inflammation*. 2016;39(3):964–973. doi:10.1007/s10753-016-0311-9
29. Xiao Y, Xu Y, Liu X, et al. Simultaneous rosiglitazone release and low-density lipoprotein removal by chondroitin sodium sulfate/cyclodextrin/poly (acrylic acid) composite adsorbents for atherosclerosis therapy. *Biomacromolecules*. 2024;25(5):3141–3152. doi:10.1021/acs.biomac.4c00241
30. Singh B, Cui K, Eisa-Beygi S, et al. Elucidating the crosstalk between endothelial-to-mesenchymal transition (EndoMT) and endothelial autophagy in the pathogenesis of atherosclerosis. *Vasc Pharmacol*. 2024;155:107368. doi:10.1016/j.vph.2024.107368
31. Du L, Long H, Wei J, et al. Xintongtai Granule: investigating the serum pharmacology and mechanisms of action against atherosclerosis. *J Chromatogr B*. 2024;1241:124165. doi:10.1016/j.jchromb.2024.124165
32. Poznyak A, Bharadwaj D, Prasad G, et al. Anti-inflammatory therapy for atherosclerosis: focusing on cytokines. *Int J Mol Sci*. 2021;22(13):7061. doi:10.3390/ijms22137061
33. Xuan Y, Yu C, Ni K, et al. Protective effects of tanshinone IIA on porphyromonas gingivalis-induced atherosclerosis via the downregulation of the NOX2/NOX4-ROS mediation of NF-κB signaling pathway. *Microbes Infect*. 2023;25(8):105177. doi:10.1016/j.micinf.2023.105177
34. Pan H, Ho SE, Xue C, et al. Atherosclerosis is a smooth muscle cell-driven tumor-like disease. *Circulation*. 2024;149(24):1885–1898. doi:10.1161/circulationaha.123.067587
35. Sun C, Li J, Li Y, et al. Circular RNA circUBR4 regulates ox-LDL-induced proliferation and migration of vascular smooth muscle cells through miR-185-5p/FRS2 axis. *Mol Cell Biochem*. 2021;476(11):3899–3910. doi:10.1007/s11010-021-04207-0
36. Alharbi KS, Fuloria NK, Fuloria S, et al. Nuclear factor-kappa B and its role in inflammatory lung disease. *Chem Biol Interact*. 2021;345:109568. doi:10.1016/j.cbi.2021.109568
37. Li L, Zhuang S, Jiang S. Muscone inhibits the progression of atherosclerotic plaques in mice aorta by inhibiting the NF-κB/p65 pathway. *Biochem Biophy Res Co*. 2024;702:149628. doi:10.1016/j.bbrc.2024.149628
38. Liu C, Wu J, Jia H, et al. Oncostatin M promotes the ox-LDL-induced activation of NLRP3 inflammasomes via the NF-κB pathway in THP-1 macrophages and promotes the progression of atherosclerosis. *Ann Transl Med*. 2022;10(8):456. doi:10.21037/atm-22-560
39. Zheng C, Ji Z, Xu Z, et al. Overexpression of miR-146a-5p ameliorates inflammation and autophagy in TLCs-induced AR42J cell model of acute pancreatitis by inhibiting IRAK1/TRAF6/NF-κB pathway. *Ann Clin Lab Sci*. 2022;52(3):416–425.